

Glacier surge propagation by thermal evolution at the bed

Tavi Murray,¹ Graham W. Stuart,² Paul J. Miller,² John Woodward,¹ Andrew M. Smith,³ Philip R. Porter,¹ and Hester Jiskoot¹

Abstract. Bakaninbreen, southern Svalbard, began a prolonged surge during 1985. In 1986, an internal reflecting horizon on radio echo sounding data was interpreted to show that the position of the surge front coincided with a transition between areas of warm (unfrozen) and cold (frozen) bed. Ground-penetrating radar lines run in 1996 and 1998 during early quiescence show that the basal region of the glacier is characterized by a strong reflection, interpreted as the top of a thick layer of sediment-rich basal ice. Down glacier of the present surge front, features imaged beneath the basal reflection are interpreted as the bottom of the basal ice layer, the base of a permafrost layer, and local ice lenses. This indicates that this region of the bed is cold. Up glacier of the surge front, a scattering zone above the basal reflection is interpreted as warm ice. There is no evidence for this warm zone down glacier of the surge front, nor do we see basal permafrost up glacier of it. Thus, as in early surge phase, the location of the surge front is now at the transition between warm and cold ice at the glacier bed. We suggest that the propagation of the front is associated with this basal thermal transition throughout the surge. Because propagation of the front occurs rapidly and generates only limited heat, basal motion during fast flow must have been restricted to a thin layer at the bed and occurred by sliding or deformation localized at the ice-bed interface.

1. Introduction

1.1. Svalbard Glaciers and Glacier Surging

Glacier surging is an internally triggered, recurrent flow instability [Meier and Post, 1969]. Slow ice flow during a prolonged (20 to >200 year) quiescent phase is followed by flow 10–1000 times faster during a short (1 to >10 year) active (or “surge”) phase. During quiescence the glacier builds up a store of ice in a reservoir zone, which is transferred down glacier during the surge phase. Surges are often associated with frontal advance of the glacier. Fast flow during the surge is considered to result from fast basal motion rather than an ice creep instability; a surging glacier becomes decoupled from its bed by trapped high-pressure water [Clarke, 1987]. It has been suggested that fast flow could be facilitated by basal sliding over a high-volume, high-pressure system of linked cavities [Kamb, 1987; Björnsson, 1998] or by

the deformation of weak saturated sediments [Clarke *et al.*, 1984]. Whatever the mechanism, basal processes are considered fundamental in initiating and maintaining glacier surging, but a paucity of observations during the active phase prevents a full understanding of the surge process.

The geographic distribution of surge-type glaciers is markedly nonuniform, on both a global scale and a local scale [Clarke *et al.*, 1986]. Surge-type glaciers are clustered in certain regions but are completely lacking from others. Svalbard is one such cluster, where we estimate the percentage of surge-type glaciers to be 13% [Jiskoot *et al.*, 1998], while others estimate the percentage to be 90% [Lefauconnier and Hagen, 1991]. Both estimates are markedly higher than the global average of <1%. Such clustering implies that environmental conditions must play a role in controlling the distribution of surge-type glaciers. In Svalbard, bedrock geology has been shown to be one important control [Hamilton and Dowdeswell, 1996], with surging being most common where a glacier overlies shales and mudstones [Jiskoot *et al.*, 1998]. These rocks are highly erodible, and glaciers that overlie them are likely to have deformable (soft) rather than hard bedrock beds. Furthermore, surge-type glaciers in Svalbard are known to be associated with enhanced englacial debris contents [Clapperton, 1975], presumably because of their sedimentary beds. The processes by which the majority of this sediment is incorporated are thought to reflect basal conditions

¹School of Geography, University of Leeds, Leeds, England.

²School of Earth Sciences, University of Leeds, Leeds, England.

³Physical Sciences Div., British Antarctic Survey, Natural Environment Research Council, Cambridge, England.

Copyright 2000 by the American Geophysical Union.

Paper number 2000JB900066.
0148-0227/00/2000JB900066\$09.00

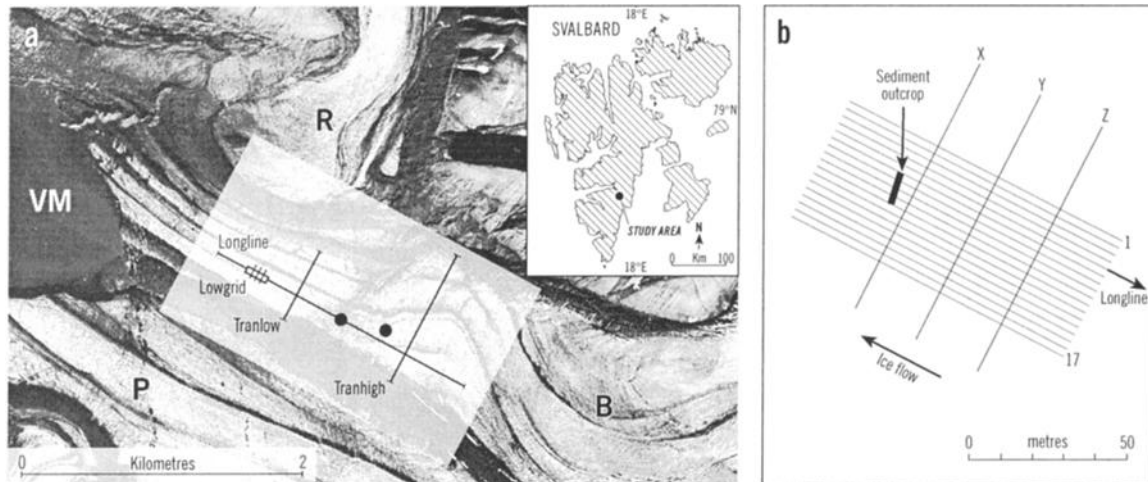


Figure 1. Bakaninbreen, Svalbard. (a) Location map and GPR lines. CMP surveys were undertaken at the crossing points of Longline and Tranlow (low CMP) and Longline and Tranhigh (high CMP). The dots mark the location of thermistor strings closest to Longline. B, Bakaninbreen; P, Paulabreen; R, Ragna-Mariebreen; VM, Van Mijenfjorden. (b) Pseudo-3-D grid layout for Lowgrid. Air photo (taken 1990): S90 6825 Norsk Polarinstittutt ©.

beneath the surging rather than deposition during the quiescent phase of the glaciers [Clapperton, 1975].

Bakaninbreen is a 17-km-long surge-type glacier situated at the head of Van Mijenfjorden in southern Svalbard (Figure 1). The glacier underwent a prolonged surge during 1985–1995 [Murray et al., 1998]. The bed of the glacier consists of a layer of sediments at least 1–3 m thick [Porter et al., 1997], which overlies erodible sandstone and friable mudstones. This sediment is a mixture of marine muds and tills [Ham-brey et al., 1996]. This might suggest a soft-bed surge mechanism operates on Bakaninbreen, as has been suggested to operate elsewhere in the Svalbard archipelago [Jiskoot et al., 1998]. Murray et al. [1997] used ground-penetrating radar (GPR) to image englacial features within the surge front of the glacier. This paper describes additional, more extensive, and higher-quality two-dimensional (2-D) GPR data acquired in 1996 and 1998 in early quiescence, new 3-D control on the geometry of englacial reflectors and concentrates on features seen at the glacier bed to constrain models of the surging process.

1.2. Surge of Bakaninbreen

Bakaninbreen began surging during 1985, and a steep surge front developed where fast moving surging ice met stagnant ice down glacier (Figure 2a). The front was 25 m high during the early stages of the glacier surge and up to 60 m high during the later stages of glacier surging [Murray et al., 1998]. The annual propagation of the surge front was $1.0\text{--}1.8\text{ km yr}^{-1}$ during 1985–1989 and then fell considerably over the period 1989–1995 (Figure 2b). By 1994–1995 the surge front had effectively ceased propagation $\sim 1.8\text{ km}$ from the glacier ter-

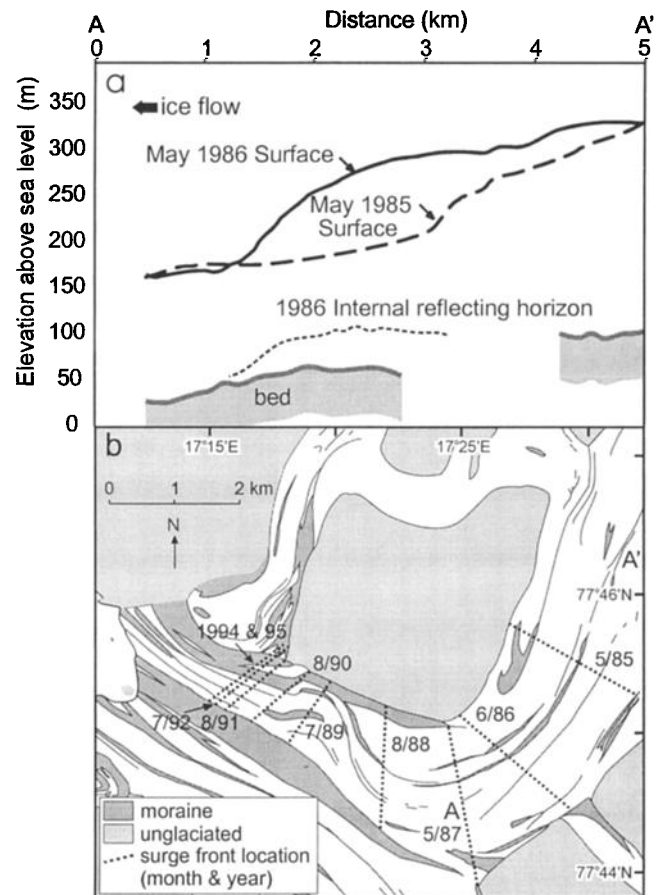


Figure 2. Propagation of surge front at Bakaninbreen [from Dowdeswell et al., 1991; Murray et al., 1998]. (a) Propagation of surge front 1985 to 1986. Bed profile was determined from radio echo sounding undertaken in 1985 and 1986. (b) Surge front position (1985–1995) from aerial photography and ground surveying.

minus (Figure 2b). The front margin of Bakaninbreen did not advance as a result of this surge.

Radio echo sounding at 60 MHz, undertaken in 1986 while surging was at its height, shows the existence of an internal reflecting horizon (IRH) located beneath the surge front (Figure 2a). Internal reflecting horizons imaged at frequencies such as these have been interpreted elsewhere as resulting from the boundary between cold and temperate (warm) ice, that is, ice which is at the pressure-melting point [e.g., *Bamber, 1988, 1989; Hagen and Strang, 1991; Björnsson et al., 1996; Ødegard et al., 1997*], and this is also believed to be the case on Bakaninbreen. In 1986, during full surge conditions this boundary intersected the bed at about the location of the surge front. It therefore appears that in 1986, cold basal ice down glacier of the surge front was frozen to its bed, whereas up glacier of the surge front, the glacier was warm-bedded.

2. Data Collection

We have collected more than 10 km of 100 MHz center-frequency GPR data at Bakaninbreen during field seasons in summer 1996 and spring 1998. The radar used in all of these surveys was a PulseEKKO 100 ground-penetrating radar manufactured by Sensors and Software Inc., Mississauga, Ontario, Canada. Three types of survey were undertaken: common midpoint surveys to determine velocity structure; 2-D common offset profiles for large-scale coverage of the glacier bed; and pseudo-3-D common offset grids for detailed imaging of englacial structures. A summary of all of the surveys discussed in this paper is given in Table 1, and their locations are shown in Figure 1.

During a common midpoint (CMP) survey the antennae are moved apart repeatedly in opposite directions

by an equal offset, such that the central image point remains constant. Such surveys are used to determine the velocity of propagation of the radar energy from the move-out of reflections, assuming near-horizontal interfaces. One pair of CMP surveys orientated along and perpendicular to the ice flow direction was collected in summer 1996, and one was collected in spring 1998 (Figure 1 and Table 1).

Common offset (CO) surveys are analogous to seismic reflection profiles. The transmitter and receiver were fixed 2 m apart on a small sledge and moved progressively along the survey lines (Table 1). Our surveys were undertaken with the transmitting and receiving antennae orientated parallel to one another and perpendicular to the orientation of the survey lines. This orientation minimizes reflections from offline because the radiation pattern has its widest energy footprint in the H plane, which is perpendicular to the antenna axis [*Arcone, 1995; Arcone et al., 1995*]. For accuracy over steeply dipping features and for comparison with the known position of surface-mapped features, our surveys were undertaken in stop-and-collect, rather than continuous collection mode.

The common offset data (Figure 1 and Table 1) consisted of (1) a line orientated along the ice flow direction ("Longline"), (2) two transverse lines, one situated up glacier and one down glacier of the surge front: "Tranhigh" and "Tranlow", respectively, and (3) a pseudo-3-D grid of 17 closely spaced longitudinal and three transverse CO lines ("Lowgrid"; Figure 1b) positioned over an emergent sediment feature that stood ~0.3 m above the snow lying on the glacier surface. Sediment was sampled from the portion of the feature lying above the snow level. This sediment contained striated and rounded clasts.

On a typical valley glacier, maximum subsurface topographic relief occurs in the cross glacier direction. However, at Bakaninbreen, GPR surveys by *Murray et al. [1997]* showed that the bed topography near this location varies only gently in this direction. Hence the majority of the CO lines in 1998 were orientated approximately in the ice flow direction.

3. Data Processing

Data processing was undertaken using GRADIX version 1.10 software. The processing stream for common offset lines was optimised on lines from Lowgrid, and then the same data processing was applied to all lines. Figure 3 summarizes the details of the data processing sequence. In common with some other radar surveys, our raw data show a repetitive horizontal banding which is coherent across a radar section [*Conyers and Goodman, 1997*], attributed to ringing in the antennae. Background removal was used to reduce this noise common to all traces (Figure 3). Migration attempts to move dipping reflectors into their true subsurface position and collapses diffractions. Two-dimensional migra-

Table 1. Summary of Survey Details of Data Discussed in This Paper

Survey	Date of Survey	Survey Details
Longline	March–April 1998	2000 m CO line
Lowgrid	March–April 1998	17x160 m lines 3x90 m tie-lines
Tranlow	March–April 1998	540 m CO line
Tranhigh	March–April 1998	1040 m CO line
High CMP	March–April 1998	up glacier
High CMP	March–April 1998	cross glacier
Low CMP	Aug. 1996	up glacier
Low CMP	Aug. 1996	cross glacier

The location of each survey is shown on Figure 1. All surveys used 100 MHz antennae, which were spaced 2 m apart during common offset (CO) surveys. The sampling interval was 0.8 ns. At each station, 64 samples were averaged to improve the signal-to-noise ratio of the data. Station spacing for CO surveys and outstep for common midpoint (CMP) surveys was 0.5 m. The line separation within Lowgrid was 2.5 m.

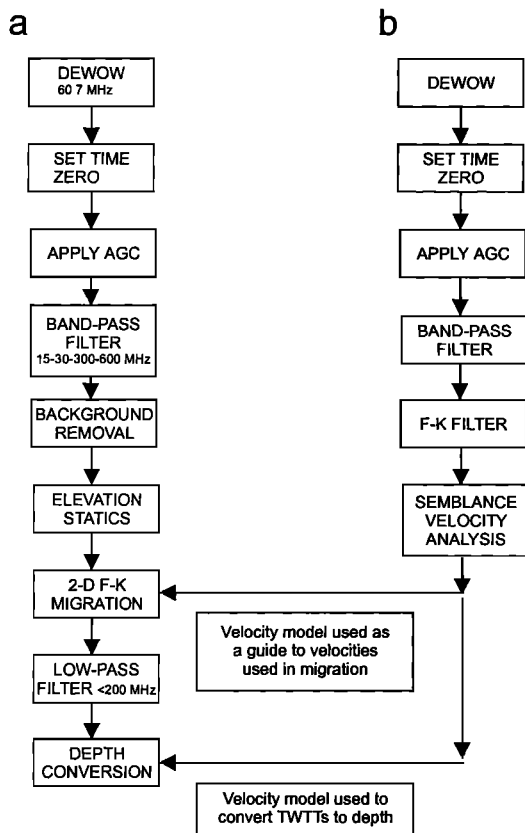


Figure 3. Summary of processing sequence applied to (a) common offset data and (b) common midpoint data. TWT, two-way travel time. Background removal reduces noise that is coherent across a section. A window is defined, and the common signal between sum of all traces in this window and the current trace is considered noise and subtracted from the current trace. The time window that this operator was applied over was limited to leave the air and ground wave and the basal reflector unattenuated.

tion algorithms assume that profiles are oriented along the true dip direction of features and that none of the energy in the section originates from outside the plane of the profile. Otherwise, reflectors to the side would be mapped with the incorrect geometry below the profile. Englacial features on our surveys fit these assumptions reasonably well as they are orientated approximately transverse to the ice flow direction and hence perpendicular to the lines. Confirmation of this comes from interpretation of the pseudo-3-D grid (Lowgrid) presented later. Migration velocities were determined from the velocity analysis of the CMPs. A velocity of 0.167 m ns^{-1} at the surface, interpolated down to 0.162 m ns^{-1} at the main subsurface reflection, was found to produce a focussed migrated image. Below this reflection (assumed to be close to the glacier bed), a constant velocity of 0.162 m ns^{-1} was used in the migration. A lower velocity is typical of those associated with subglacial materials (rock, unfrozen or frozen till; Table 2). Incorporating this reduced velocity at depth into the velocity model improved the resolution of strong, linear reflections seen deeper in the section.

Prior to velocity analysis, data from CMP surveys were processed in a similar way to the common offset lines (Figure 3). An additional F-K filter was applied, which reduces aliased energy and noise [Yilmaz, 1987, p. 69], to optimize the accuracy and resolution obtained in velocity analysis.

4. Results From the CMP Surveys

The first arrival on a CMP survey is the air wave traveling directly between the transmitter and receiver. Typically, this wave is followed by a single ground-coupled wave traveling through the surface medium (ice wave), and this is the case for our summer CMP sur-

Table 2. Dielectric Permittivities and Velocity for Materials Common in the Glacial Environment

Material	Velocity, m ns^{-1}	Dielectric Coefficient
Air	0.300	1
Snow	0.194–0.252	1.2–2.0 (dry) 1.5–3.3 (wet)
Cold ice	0.167–0.170	3–4
Warm ice	0.14–0.16	1.9–2.1
Water	0.033	80
Sediment-rich ice	0.122 ^a	6
Permafrost	0.12–0.15	4–6.3 ^a
Till (porosity=0.15)	0.087 ^a	12
Till (porosity=0.3)	0.071 ^a	18
Shales and mudstone	0.09	5–15

Sources are: Bogorodsky et al. [1985], Jones [1987], Davis and Annan [1989], Macheret et al. [1993].

^aCalculated from $v = 0.3/\sqrt{\epsilon_r}$, which is applicable to low loss media only.

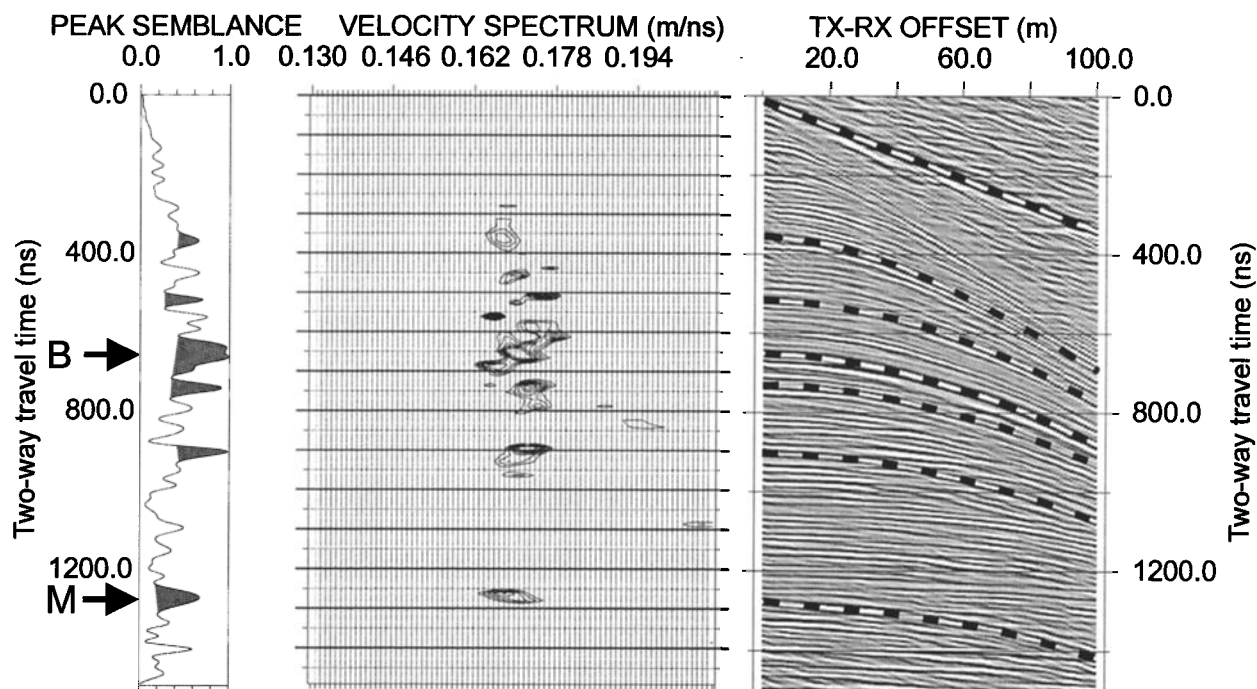


Figure 4. Semblance plot of CMP survey down glacier of surge front. The fit to a hypothetical hyperbolic trajectory calculated from the normal move-out equation is measured by the semblance. The semblance is large when a coherent event is present and is also sensitive to the event magnitude. Thus strong events will exhibit high values of semblance, weak events moderate semblance values and incoherent energy very low semblance. TX, transmitter; RX, receiver. The basal reflector (B) and its multiple (M) are indicated.

veys. However, in the surveys collected in spring, when the glacier surface was covered by a meters-thick layer of snow, a third wave can be seen traveling at a higher velocity than that for glacier ice. We interpret the three waves in the spring surveys as an air wave, a wave traveling through the surface snow layer (snow wave), and a wave traveling in some combined path through the snow and the glacier ice surface (combined wave). The velocity of this combined wave is greater than that of the summer ice wave. As we are uncertain about the exact path of this wave, we take the velocity in the surface layers of ice from the summer (1996) CMP surveys only. Graphs of arrival time against offset for the air wave, winter snow wave and summer ice wave have linear slopes which can be used to calculate their velocity of propagation. Mean values from all surveys were air wave $0.300 \pm 0.003 \text{ m ns}^{-1}$; snow wave $0.230 \pm 0.003 \text{ m ns}^{-1}$; and ice wave $0.170 \pm 0.003 \text{ m ns}^{-1}$.

Within the resolution of the technique no velocity anisotropy was seen; to the first order the velocity field seems to be dependent on depth in the ice. In Figure 4 we present the results of the velocity analysis of the CMP oriented across the ice flow direction and situated down glacier of the surge front (Figure 1a). With such an orientation, we expect most reflecting interfaces to be subhorizontal. Semblance analysis [e.g., *Sheriff and Geldart*, 1995, p.288] was used to determine the normal move-out velocities of reflections at different depths

within the glacier (Figure 4). Semblance is a measure of the coherence of hyperbolic reflection energy at a particular normal move-out velocity. The velocities picked from the highs of the semblance plots can be converted to interval velocities using Dix's equation [e.g., *Sheriff and Geldart*, 1995, p. 130] provided the small-spread approximation holds: that is, the depth to the reflector is very much greater than the distance between the antennae.

Down glacier of the surge front, the radar velocity is relatively constant at $0.167\text{--}0.170 \text{ m ns}^{-1}$ down to $\sim 680 \text{ ns}$ (zero offset). At greater times, there are few reflections visible on the semblance plot (Figure 4). The reflection at 1280 ns is a multiple of that at 640 ns . Similar results are seen on the CMP up glacier of the surge front, although there is some suggestion of a reduction of velocity with depth, with velocity dropping to 0.165 m ns^{-1} at two-way travel times $>1420 \text{ ns}$. One plausible explanation of such a velocity drop would be the presence of warmer basal ice (Table 2). Further evidence for this will be presented in sections 8.2 and 9.3. For simplicity, a constant ice velocity of 0.167 m ns^{-1} was used in all englacial depth conversions and is assumed in discussions of the geometry of englacial features. For subglacial material a velocity of 0.150 m ns^{-1} was used (Table 2).

The progressive separation in time of the air wave from the corresponding snow and ground waves as the

antennae are moved apart during CMP surveys allows determination of the phase of the wavelet transmitted into the ice. This is necessary in order to determine the relative dielectric permittivity (dielectric coefficient) across reflecting interfaces [Arcone *et al.*, 1995]. Examination of the CMP surveys shows that the wavelet of the air wave has phase progression: positive-negative-positive, shaded black-white-black (b-w-b) on plots in this paper. The waveforms of the snow and ice waves, on the other hand, have traversed the ice surface and have an opposite polarity, appearing white-black-white (w-b-w) in the plots. Reflections from interfaces where the dielectric coefficient decreases (velocity increases) will not be phase-shifted relative to the ice wave and will appear w-b-w in sections, whereas reflections from interfaces where the dielectric coefficient increases (i.e., those for which the velocity decreases) will be phase-shifted relative to the ice wave by close to 180° and will appear b-w-b in sections (Figure 5). This enables some verification of the type of material contrast producing the reflections in the common offset profiles. Table 2 gives dielectric coefficients and velocities for common glacial materials.

5. Results From the Longline CO Profile

The main features of the processed section of Longline (Figure 6) include the following:

1. A strong subhorizontal reflection (B) is continuous across the majority of the section at a two-way travel time of 490–1550 ns (equivalent to 41–129 m of ice). This reflection is shallowest at the base of the surge front and deepens both up and down glacier (Figure 6). It is deepest at 2000 m distance along the line.

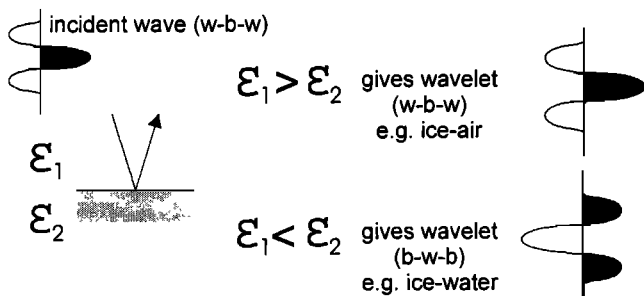


Figure 5. GPR wavelet polarity resulting from a subsurface reflection between materials with different dielectric coefficients (e.g., Table 2). The incident wave has polarity w-b-w. The phase shift, Λ , of the reflected wave in (b) is not exactly as shown; for example, ice-water $\Lambda=179^\circ$; ice-wet till (porosity=0.15) $\Lambda=164\text{--}177^\circ$; ice-wet till (porosity=0.30) $\Lambda=167\text{--}176^\circ$ [Jones, 1987]. However, the angles are close enough to 0° or 180° that the difference in waveform cannot be distinguished.

Using borehole control, Murray *et al.* [1997] interpreted a similar reflector as the top of a layer of basal ice. This reflection is by far the strongest and most extensive arrival seen on all our radar data. We also believe, from borehole data, that it originates somewhere within a few tens of meters of the glacier bed. Because of this, we will refer to this reflection as the “basal” reflection. However, we stress that it is not necessarily the true bed of the glacier. Indeed, our interpretation that follows shows that this is not the case. We believe that it represents the interface between relatively clean glacier ice and a lower layer of basal ice containing a significant concentration of sediment. The true glacier bed, defined by a present or past *décollement* surface, lies somewhere below the basal reflection, and it may, or may not, be associated with a later arrival on our radar data.

The basal reflection (B) has a reversed phase (b-w-b), which is consistent with this interpretation (Table 2 and Figure 5). It is often disrupted or missing at the base of englacial features that dip up glacier (e.g., at 564 m on Figure 6b). Typically, the basal reflection appears remarkably flat and is a single wavelet. Some variation in time does occur, for example, “bumps” below the surge front at 150 m and 420 m, and a long-wavelength trough (T in Figure 6a) between 1700 and 1860 m. The first multiple of this reflection can also be seen for most of the region down glacier of the surge front, marked M on Figure 6 (this is energy that has been multiply reflected between the glacier’s surface and base).

2. A zone of increased scattering immediately above the basal reflection can be seen up glacier of the surge front (e.g., S and S1 in Figure 6a). The top of this zone is diffuse and marked by a large number of hyperbolae that are incompletely collapsed by migration. The zone is thickest up glacier (1700–1800 m along the profile), varying in two-way travel time between 370 and 680 ns (31–57 m thick). The zone almost doubles in thickness over the trough in the basal reflection (T) but pinches out down glacier and can no longer be discerned down glacier of 1080 m. It is noted here, for discussion in section 10.1, that the top of this zone is similar in location and depth, relative to the present surge front, to the internal reflecting horizon seen in the 1986 radar data (Figure 2a), although the zone varies in thickness more than the 1986 early surge phase internal reflecting horizon.

3. A series of coherent englacial reflections dip up glacier at around $21^\circ\text{--}35^\circ$ (three examples are marked E in Figure 6), a few of which intersect the glacier surface. From the data collected in 1996, Murray *et al.* [1997] interpreted these structures as sediment entrained along faults. Down glacier of the surge front (down glacier of 1060 m in Figure 6b), there are more than 19 of these features, at least two of which appear to outcrop at the glacier surface (at 680 and 290 m). These features are at their most prominent immediately up glacier of the surge front (1050–1300 m, Figure 6a).

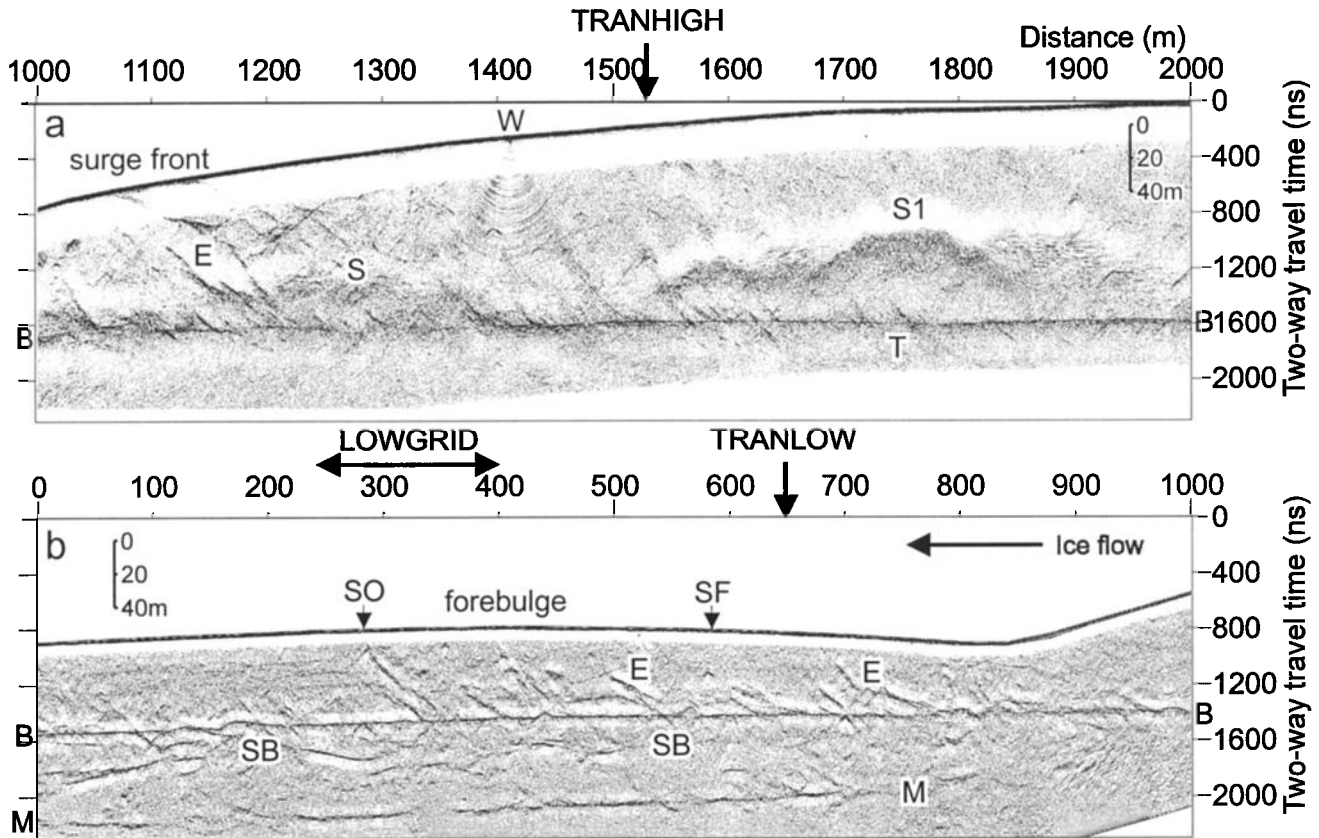


Figure 6. Longline GPR profile. The topography of the forebulge can be clearly seen with its maximum at 350 m. The surge front begins at ~830 m. B, basal reflection; W, wire to instrument at glacier bed; S, scattering zone; T, trough in basal reflection where scattering zone increases in thickness; E, shallowly dipping englacial features; SO, sediment outcrop on Lowgrid; SB, subglacial reflections; SF, steeply dipping englacial feature; M, first multiple of basal reflection. The white ghosting effect around strong reflections and following the air wave is caused by the AGC gain function used. Note that the AGC gain changes at 1000 m. The vertical scale is the same for the whole figure, but the time origin differs between the two sections. The depth scale bar shown assumes a propagation velocity of 0.167 m ns^{-1} .

4. A number of steeper up glacier dipping features are picked out by an almost vertical line of diffractions (e.g., SF on Figure 6b). This type of feature is less common than the shallow features, and there are only four clear examples on the lower portion of the glacier, one of which is situated within Lowgrid and is described below.

5. A series of linear features beneath the basal reflection occur down glacier of the surge front (e.g., SB on Figure 6b). Some of these features are roughly horizontal, others dip up or down glacier. They are often strong which in some cases may result from constructive interference within a thin layer. Two major reflection levels can be seen, both of which are fairly continuous, although in places they are picked out by a series of reflections interspersed with gaps. Both fade ~200 m down glacier of the surge front and cannot be identified up glacier of this. While these reflecting horizons appear to originate from below the basal reflector, it is not possible from single 2-D lines to exclude the possi-

bility that these reflections are from englacial positions offline. However, results of 3D visualization (presented in section 6) show that they originate from beneath the basal reflector.

6. Results From Three-Dimensional Visualization of Lowgrid

The $40 \times 160 \text{ m}$ area covered by Lowgrid (Figure 1) includes a shallowly dipping, englacial feature that cropped out at the glacier surface (Figure 7). Samples from the outcrop revealed that the sediments are similar to others collected nearby, which have been interpreted as being basal in origin [Hambrey *et al.*, 1996]. Lowgrid also has a clear, strong basal reflection, as seen on Longline, and some of the clearest subbasal reflections (e.g., F and G in Figure 7) as well as a steeply dipping englacial feature.

The visualization of Lowgrid in three dimensions provides a detailed analysis of the spatial variation of the

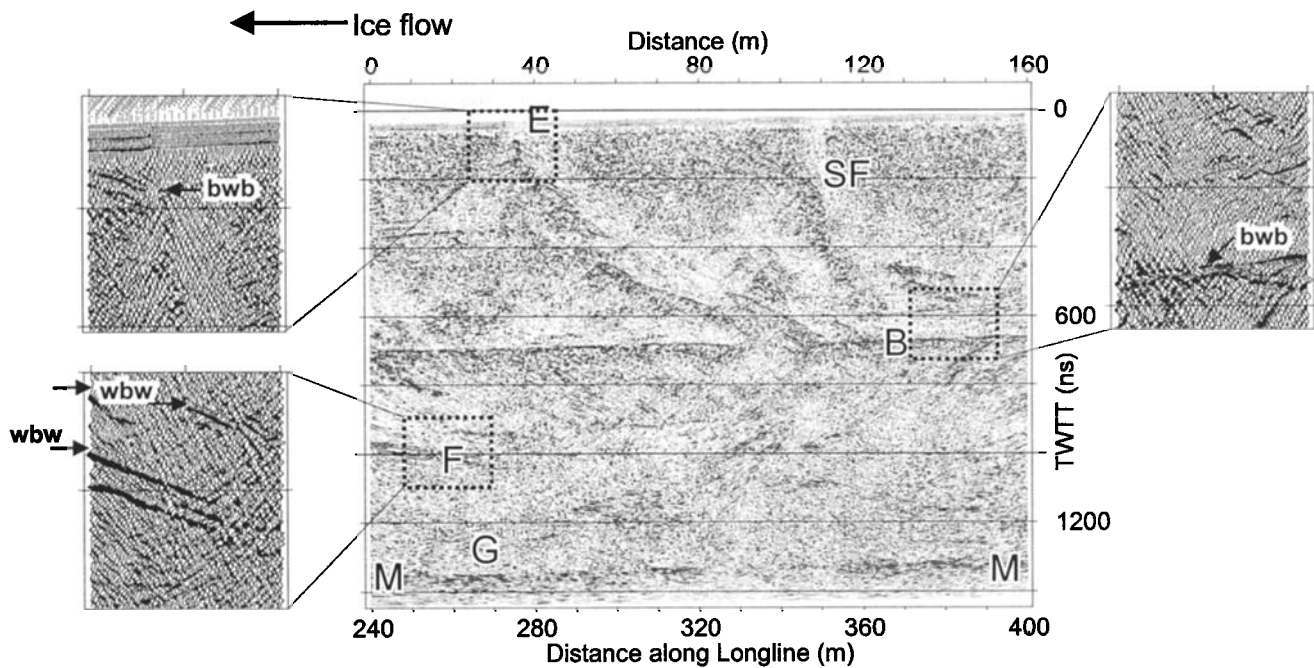


Figure 7. GPR section from Lowgrid, line 1. E, shallow dipping englacial feature; B, basal reflection; SF, steep englacial reflection; F, shallow subbasal reflection; G, deep subbasal reflection; M, first multiple of basal reflection. Enlargements show (clockwise from top left): (1) Basal reflection (b-w-b). (2) Top of “thrust” feature (which does not appear to outcrop on this line). The top of the feature has a b-w-b reflection. (3) Subbasal features (w-b-w). TWTT, two-way travel time.

outcropping sediment feature and the associated basal and subbasal reflections. In particular, the 3-D variation of the subbasal reflections on the down glacier and cross glacier oriented lines allows assessment of whether this energy is from depths below the basal reflector or originates from targets located within the ice but out of the plane of individual lines. Furthermore, the assumed two dimensionality of the structures can be assessed to confirm whether the 2-D migration algorithm used in processing the lines was satisfactory. The letters below refer to features identified in Figure 7 and Figure 8.

6.1. Basal Reflector B

The strong basal reflection shows no major variation in depth across the grid (Figure 8a). The two-way travel time to this reflector is 670–680 ns (53.4 ± 0.5 m). The reflection at ~ 1340 ns (M on Figure 7) is interpreted as a multiple of this basal reflection.

6.2. Shallow Dipping Englacial Feature E

The englacial feature that dips up glacier at a shallow angle is not continuous but appears to be composed of segments (Figure 8a). The feature disrupts the basal reflection. The reflection at the top of this feature has phase b-w-b (Figure 7), consistent with an interface across which the dielectric coefficient increases, e.g., a boundary between ice and sediment or ice and sediment-

rich ice (Table 2). Although discontinuous, this reflection can be identified across the whole grid, being strongest on line 1 and fading toward line 17. It has a concave upward geometry, steepening from $\sim 30^\circ$ close to the basal reflection to $\sim 45^\circ$ toward the glacier surface. The feature is not orientated directly cross glacier but is skewed slightly so that its base is ~ 5 – 10 m farther down glacier on the northern side of the glacier. The locations where this feature appears to intersect the surface on some of the GPR lines (Figure 8a) agree well with where the sediment outcrop was mapped at the snow surface (Figure 1). We suggest that the feature delineates a fault within the glacier ice. This is supported by the change in the angle of a radar reflection fabric at the feature. Up glacier of the feature weak reflectors dip down glacier at an angle that is steeper than the ice surface topography. At the dipping feature, however, these reflectors become abruptly more horizontal.

6.3. Steeply Dipping Englacial Feature SF

The steeply dipping feature is difficult to image using a reflection technique. However, it appears to comprise a series of diffractors with dip angles of 60° – 90° (Figure 8b), which can be correlated for ~ 15 m across the grid before fading into a few isolated diffractors. It does not appear to intersect the glacier surface.

6.4. Shallow Subbasal Feature F and Deeper Subbasal Feature G

The shallower of the two subbasal features correlates across the grid varying in depth below the basal reflection between 5 and 22 m (Figure 8c). It appears to dip at an angle of $\sim 20^\circ$ cross glacier toward Ragna-Mariebreen (Figure 1). The deeper of the subbasal features also correlates across grid, varying in depth (below the basal reflection) between 17 and 35 m (Figure 8d). It dips toward Ragna-Mariebreen at an angle of $\sim 24^\circ$. The continuity of these features between lines, their appearance on the cross lines, and the fact that they tie between cross and down glacier orientated lines supports the assertion that while some reflections appearing at travel times greater than the basal reflection may originate from offline, these deeper reflectors are, in fact, situated below the basal reflector.

7. Results From Tranhigh and Tranlow CO Profiles

The processed GPR sections from Tranhigh and Tranlow CO lines show very similar features to those de-

scribed in the previous sections. The basal reflection is strong and clear with a b-w-b polarity. The scattering zone can be seen on Tranhigh but not on Tranlow. Conversely, clear subbasal reflections at a similar depth to those on Longline and Lowgrid can be seen on Tranlow but not on Tranhigh. On Tranlow, these subbasal features can be traced across virtually the full width of the glacier, and there is no evidence that they cross the basal reflector.

8. Evidence for the Nature of Reflectors

8.1. Drilling Depths: Nature of the Basal Reflector

We drilled a total of 98 boreholes with a hot water drill on Bakaninbreen during 1994 and 1995 summers in order to install instrumentation at the glacier bed [e.g., Porter *et al.*, 1997]. The depth at which each hole terminated was measured on the hose of the drill. Each hole was drilled to the maximum depth possible, and the drill was run for up to an hour if the hole appeared to terminate englacially. The 34% of holes that terminate within the body of ice are believed to be the result of

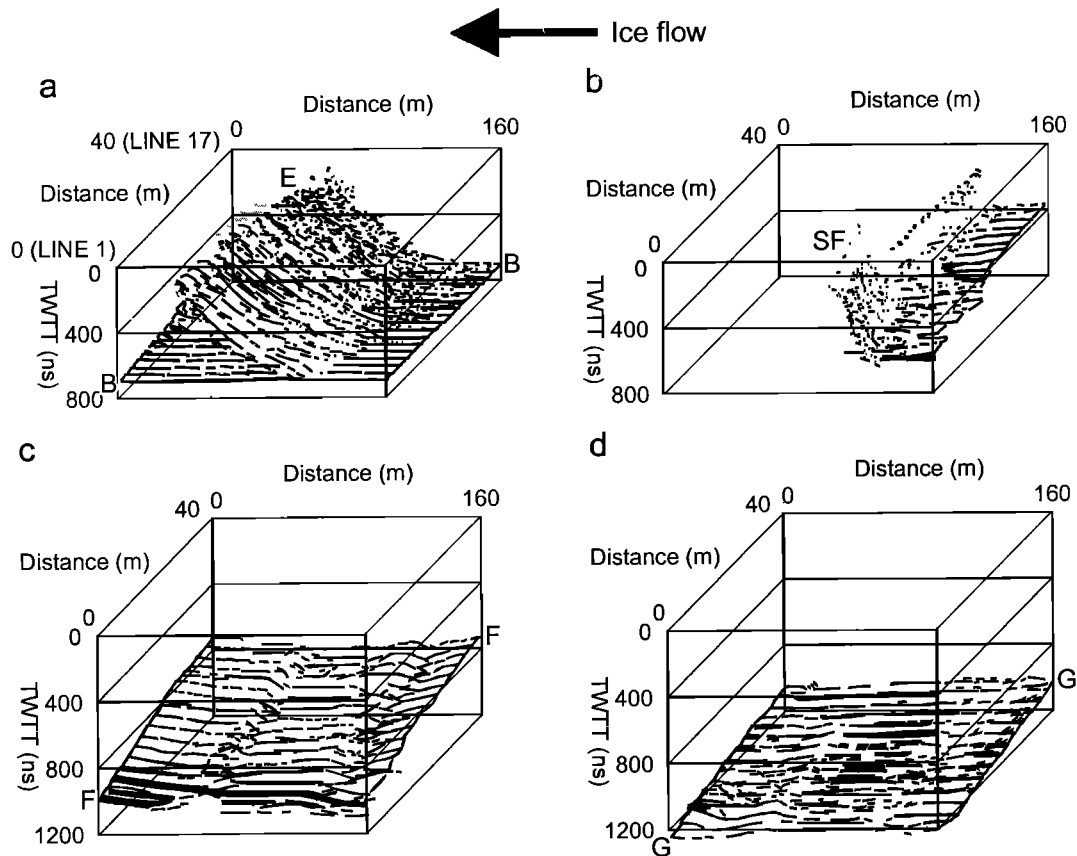


Figure 8. Three-dimensional structure of the major reflectors of Lowgrid. (a) Low-angle feature and “basal” reflector. Black lines are englacial; grey lines intersect the glacier surface. (b) Steep englacial feature. (c) Shallow subbasal reflector. (d) Deep subbasal reflector. TWTT, two-way travel time.

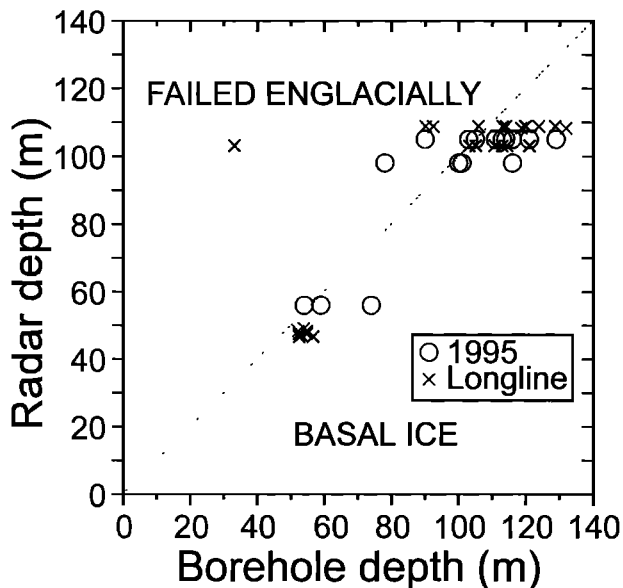


Figure 9. Comparison of the depths of boreholes within 10 m of radar lines with the GPR-derived depth to the basal reflector. The dashed line divides holes where the borehole depth is less than the depth of the basal reflector (assumed to terminate englacially due to sediment inclusions) from those where the borehole depth is greater than that to the basal reflection. The latter holes are more common, and this is thought to result from the basal reflection occurring at the top of a layer of sediment-rich basal ice. The deepest boreholes are believed to represent the true depth of the glacier. Errors on borehole and radar depths are estimated to be better than ± 0.5 m. All radar depths assume the velocity of propagation is 0.167 m ns^{-1} . Crosses show data from Longline; circles show the data from GPR lines surveyed in 1995.

significant volumes of sediment diffusing the drill jet [Murray *et al.*, 1997]. On removing the hose from some of the longest of these holes the drill stem and hose would be coated in sediment to a height of up to 3 m.

Several of the boreholes lay within 10 m of the later position of Longline. There is some uncertainty in comparison of borehole depths and those determined from 1998 radar surveys because of the loss of ice during two (for 1995 holes) or three (for 1994 holes) summers between drilling and the GPR survey (the melt rate on the glacier was measured as $\sim 2.4 \text{ m yr}^{-1}$, unpublished data from our 1994 and 1995 field seasons) and because of the presence of unknown and probably varying depth of snow along the GPR lines (best estimate from a snow pit dug to the ice surface is 2.5 m of snow). As a result, the borehole depths could overestimate glacier thickness (as compared to the later GPR data) by ~ 2.4 –5 m. Even with this degree of uncertainty, the deepest boreholes are consistently deeper than the depth to the basal reflection (Figure 9) by 3–10 m down glacier of the surge front and 8–20 m up glacier of it. A direct comparison

of radar data acquired in 1995 [Murray *et al.*, 1997 and borehole depths of the same year also agrees with this assertion (Figure 9). This discrepancy between borehole depths and GPR depths to the basal reflection cannot be explained by nonvertical boreholes or by the use of an incorrect radar velocity in the depth conversion [Murray *et al.*, 1997]. We interpret these results to suggest that the basal reflector is the top of a layer of sediment-rich basal ice 3–20 m thick, rather than the base of the glacier itself. This layer appears to approximately double in thickness above the surge front, which is exactly as would be expected if the $\sim 100\%$ increase in glacier thickness at the surge front results largely from longitudinal compression and vertical extension [Murray *et al.*, 1998].

8.2. Nature of the Scattering Zone Up Glacier of the Surge Front

We suggest that the scattering zone imaged up glacier of the surge front (Figure 6a) represents the top of a zone of warm ice, as found elsewhere in polythermal glaciers, including others in Svalbard [e.g., Björnsson *et al.*, 1996]. The propagation velocity of electromagnetic radiation decreases with increased water content [e.g., Macheret *et al.*, 1993]. Since warm ice has a higher water content than cold ice, we expect this scattering region to have lower velocities than cold ice. Two lines of evidence support this:

1. Lower normal move-out velocities occur at the basal reflection from the CMP up glacier of the surge front. We assume a cold ice velocity of 0.167 m ns^{-1} at the location of the up glacier CMP surveys (1524 m along Longline). With these values the lowest velocity from semblance plots of 0.165 m ns^{-1} (Table 1) suggests a glacier structure consisting of ~ 102 m of cold ice underlain by a layer of ~ 12 m warm ice with velocity 0.149 m ns^{-1} at this location.

2. A depression of basal reflection on two-way travel time section that is due to increased thickness of low-velocity scattering zone. An increase in thickness of this scattering zone is seen at location S1 in Figure 6a. This is mirrored by a downwarp in the time of the basal reflector (T in Figure 6a), as would be expected if the scattering zone is of lower velocity than the surrounding ice. It is possible that this reflection geometry represents a real trough in the basal reflector. However, it would be highly fortuitous for it to occur exactly beneath the changes seen in the scattering reflection, particularly as there is little variation elsewhere on the basal reflection. Hence we consider it most likely that the basal reflector in this area is flat and that the feature T indicates a velocity pull-down effect resulting from the increased thickness of warmer ice. Assuming, therefore, that the basal reflector is flat at the location of the trough; then by measuring the change in cold ice thickness and the depression of the basal reflection, we can calculate the velocity of the warm ice and the apparent change in its

thickness. This calculation gives an increase in warm ice thickness of ~ 25 m with a velocity of $\sim 0.150 \text{ m ns}^{-1}$ at this location.

These two methods for estimating the propagation velocity in this scattering zone are in reasonable agreement. The water content of ice with a velocity of 0.149 m ns^{-1} is $\sim 3.0\text{--}4.1\%$ depending on the inclusion model used [Macheret *et al.*, 1993] and with a velocity of 0.150 m ns^{-1} is $\sim 2.8\text{--}3.9\%$. This assumes that there is no sediment within the warm ice zone, which would decrease the calculated water content.

8.3. Englacial Reflectors

Murray *et al.* [1997] interpreted these features as sediment entrained along faults within the glacier. This interpretation is consistent with the observed polarity (b-w-b) of the reflections (Figure 7). They must contain significant volumes of sediment in order to be visible on the radar sections. A minimum estimate on the thickness of each feature is ~ 0.03 times the wavelength [Sheriff and Geldart, 1995, pp. 178-179], i.e., ~ 0.052 m.

8.4. Nature of the Subbasal Reflectors

Figure 10 shows the basal reflection (B) and the region beneath it, on line 12 of Lowgrid. Subbasal re-

flections with both polarities (w-b-w and b-w-b) can be seen, for example, those marked F, G, and H. Although not continuous across the whole of Figure 10, these reflections can generally be identified across the whole of Lowgrid (see Figure 8). We discount the possibility that these deeper reflections come from bedding within underlying rocks, as their dip directions (roughly northeast) are opposite to the regional geological trends, which are to the west-southwest [Salvigsen and Wisnes, 1989].

As discussed in section 8.1, we believe that the basal reflection (B) is from the top of sediment-rich basal ice. Reflection F is clearly b-w-b, which must arise from a material with a higher dielectric coefficient than that of this basal ice. This could be due to an increase in either sediment or water content. Table 2 suggests possible materials likely to occur within the glacial environment. Permafrost, till, and rock are all possible. We discount free water on the grounds that no deeper reflections would be expected. We therefore believe that this interface is the true bed of the glacier, defined by basal motion occurring during a previous surge event (this region of the glacier never became activated during the present surge).

In Svalbard, glacier thermal regime is strongly influenced by ice thickness [e.g., Björnsson *et al.*, 1996]. At

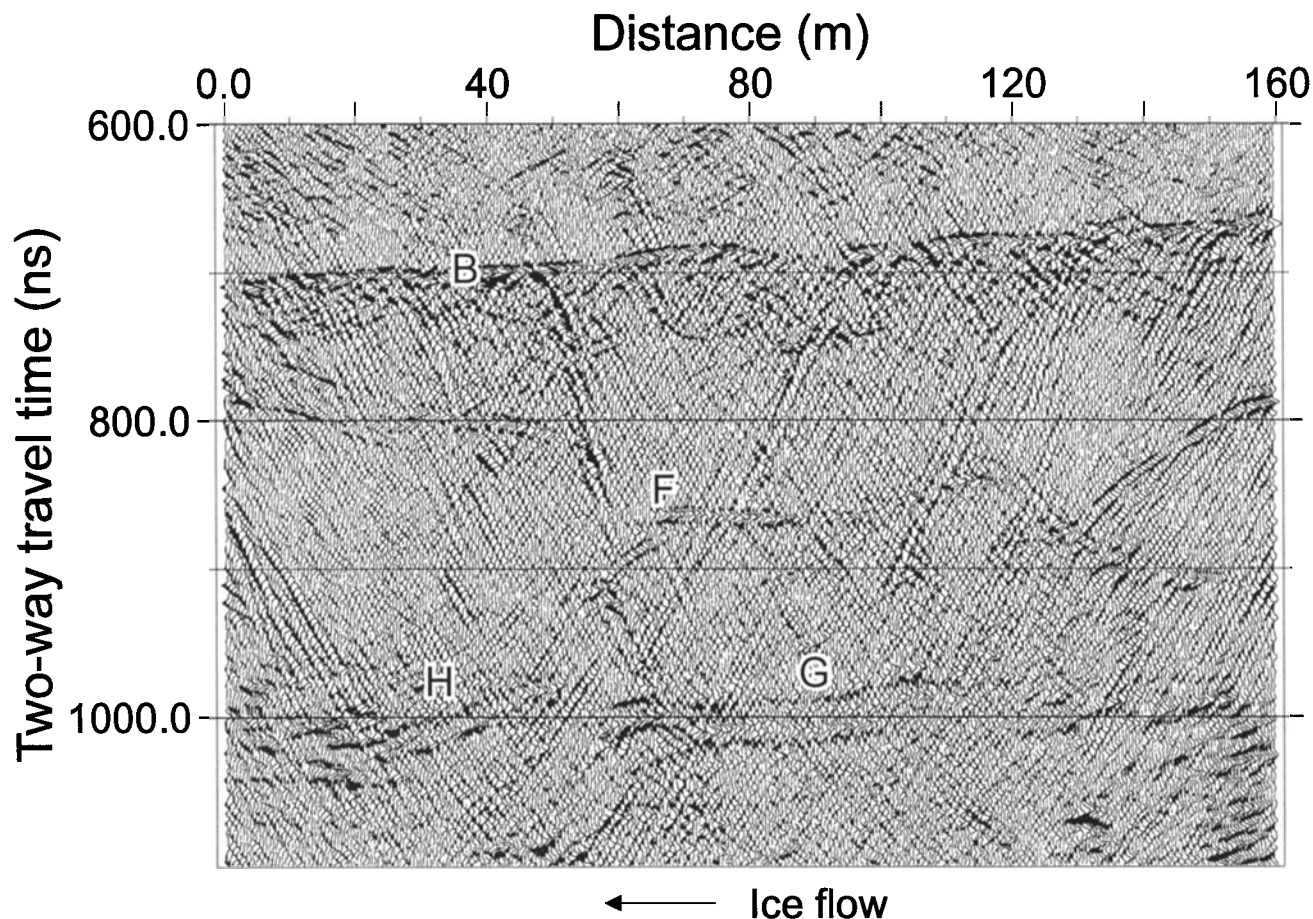


Figure 10. Detail of basal and subbasal reflections on Lowgrid, line 12. B, basal reflection; F, shallow subbasal reflection; G and H, deep subbasal reflections.

the present time, glaciers more than ~ 100 m thick are thought to be associated with warm beds, while thinner ones have cold beds. For example, Finsterwalderbreen is ~ 120 m thick and warm-based [Ødegard *et al.*, 1997], but Scott-Turnerbreen is ~ 55 m thick and cold-based [Hodgkins, 1997]. It is thus likely that in thermal equilibrium the current geometry of Bakaninbreen would be cold-bedded down glacier of the surge front and warm-bedded up glacier of it. The cold-bedded part would be underlain by a layer of permafrost. The GPR data support this thermal configuration for Bakaninbreen in two ways. First, the fact that we can see clear reflections from significant depths beneath the basal reflection down glacier of the surge front means that there must be relatively low absorption of the radar energy. Frozen subglacial materials absorb much less energy than do water-saturated ones. Second, the fact that these deeper reflections die out close to the surge front and cannot be seen farther up glacier, even though the basal reflection remains strong, suggests that there is much greater absorption of the radar energy up glacier of the surge front than there is down glacier of it. Hence we interpret reflection F as the interface between basal ice and permafrost, the true bed of the glacier. Drilling depths suggest that the thickness of basal ice in the region immediately down glacier of the surge front is 3–20 m (Figure 9). Within Lowgrid the travel time between the basal reflection, B, and the upper subbasal interface (Figure 8c) is equivalent to a thickness of 5–22 m, so this is in agreement with our interpretation.

Reflections G and H in Figure 10 are fainter than F, but their polarity can still be identified from the central lobe of the reflection wavelet. Reflection G is normal po-

larity (w-b-w), whereas H is reversed (b-w-b). Considering the overlying layer of permafrost, the most likely causes of these two reflections are clear ice lenses within the permafrost (G) and the base of the permafrost layer (or pockets of unfrozen sediment) (H). We expect ice lenses to occur within the permafrost. Hence, where the reflection from the base of the permafrost itself cannot be identified, we use the deepest ice lens reflections as a rough indication of the base of the permafrost layer. The lower interface (H in Figure 10) is situated at ~ 22 – 35 m below the basal reflector. We therefore interpret a layer of ~ 10 – 15 m of permafrost beneath the glacier. The likelihood that this is a realistic permafrost thickness, given the known glacial history of the region, is discussed in section 9.2.

9. Thermal Regime of Bakaninbreen

On the basis of the interpretation of our results described in section 8, we propose a conceptual model of the geometrical and thermal regime at Bakaninbreen (Figure 11). The following are the main features of the model:

1. Down glacier of the surge front (e.g., X on Figure 11), a vertical sequence of ~ 55 m of cold glacier ice overlies 5–22 m of sediment-rich basal ice. Beneath this there is a cold frozen bed of permafrost, 10–15 m in thickness, overlying unfrozen sediments. The shallower of the two subbasal reflectors is the base of the glacier, i.e., the interface between sediment-rich basal ice and ice-rich sediment, and the deeper reflector is the base of the permafrost layer, with clean ice rafts in places.

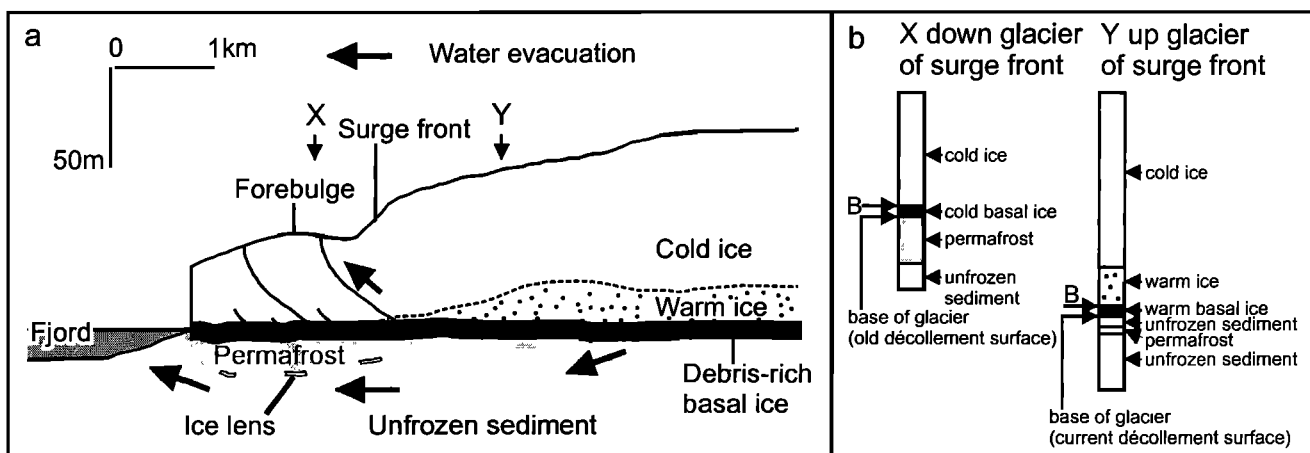


Figure 11. (a) Conceptual model of Bakaninbreen. Surge propagation will be due to glacier sliding and the deformation of a thin layer of sediments over frozen sediments. These frozen sediments act as a seal for pressurized basal water, which can only escape through groundwater flow or to the ice surface through thrusts and shear zones. (b) Schematic logs through glacier at locations X below surge front and Y above surge front. The glacier base (bed) is defined by the décollement surface across which sliding occurs or where sliding occurred in the past (e.g., during a past surge event). The basal reflection occurs at the top of the basal ice, marked B, whether this boundary is cold (down glacier of surge front) or warm (up glacier of surge front).

2. Up glacier of the surge front (e.g., Y on Figure 11), a vertical sequence of ~ 75 – 100 m of cold glacier ice overlies ~ 31 – 57 m of warm glacier ice and 7–23 m of warm sediment-rich basal ice. Beneath the ice is a thin layer of unfrozen sediment. The thickness of this layer is discussed in section 10.1.

In this model the glacier is cold-bedded in the region down glacier of the surge front and warm-bedded up glacier. We now present further discussions that support this interpretation.

9.1. Further Evidence for a Cold Glacier Bed Down Glacier of the Surge Front

Strings of thermistors were installed to the bed of Bakaninbreen during 1994, with two strings located down glacier and two located up glacier of the surge front. Measurements of ice temperature were made in 1995 approximately 1 year after installation. Those thermistors closest to the later position of Longline and down glacier of the surge front (Figure 12) showed the bed is at $-0.17 \pm 0.05^\circ\text{C}$ and is thus cold-based (the pressure melting point is $\sim -0.04^\circ\text{C}$ beneath this thickness of ice [Hobbs, 1974, p. 351]).

Plough meters and tilt cells were installed in the glacier bed during 1994 and 1995 to measure sediment properties and deformation rates [Porter, 1997]. These instruments were located both up glacier and down glacier of the surge front and show two pertinent results. First, the tilt cells up glacier of the surge front show that the sediment just below the ice-bed interface is displaced relative to the ice situated just above it [Porter, 1997]. Down glacier of the surge front, strain rates are ~ 10 times lower. Second, interpretation of data from plough meters [cf. Fischer and Clarke, 1994], which penetrated around 10–20 cm into the bed, show the effective viscosity of the basal sediments is substantially higher down glacier of the surge front (3.3×10^{12} to 6.5×10^{13} Pas) than it is up glacier (1.1×10^{10} to 4.3×10^{10} Pas) [Porter, 1997]. The former values are higher than are typically quoted for unfrozen, subglacial sediments [Murray, 1997]. This suggests that these high-viscosity sediments, down glacier of the surge front, are frozen. The latter values are more typical of unfrozen subglacial sediments.

9.2. Given the Dynamic History of Bakaninbreen, is 10–15 m a Reasonable Thickness of Permafrost?

Permafrost covers the majority of land area of Svalbard, except for thawed areas associated with lakes, large glaciers, and warm springs. The push moraine at Svea, 15 km from Bakaninbreen down Van Mijenfjorden, which is thought to represent a surge of the Paulabreen-Bakaninbreen complex 500–600 years ago, is now underlain by permafrost >100 m in thickness, and this permafrost is currently aggrading [Gregersen, 1988].

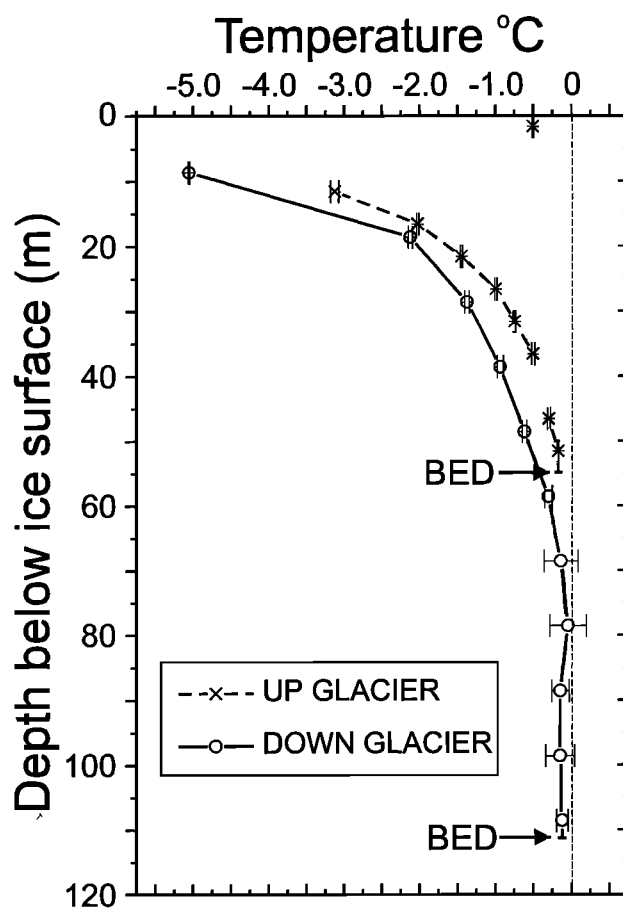


Figure 12. Temperature-depth profile measured on thermistors during 1995 one year after installation. One thermistor string (cross) was installed in a hole drilled down glacier of the surge front and indicates a cold bed, the other (circle) up glacier of the surge front, which suggests that there may be up to 40 m of warm ice at this location.

In common with many glaciers in Svalbard, Bakaninbreen has been retreating over the last few centuries. Air photographs show that there has been 1.0–1.4 km of retreat between 1977 and 1990 [Dowdeswell et al., 1991; Murray et al., 1998], and over the last 500–600 years the glacier is thought to have retreated ~ 14.5 km [Punning et al., 1976]. On the basis of the observation of trim lines on the valley walls, it is reasonable to assume that this retreat has been associated with substantial thinning of the glacier. We believe that the region down glacier of the 1990 surge front is cold-bedded and underlain by a layer of permafrost. However, it is very likely that the glacier was warm-bedded in this region sometime in the last 500–600 years, when the ice was considerably thicker. There will be some lag between the loss of ice and the development of permafrost, and so in order to ascertain whether the thickness of permafrost our interpretation requires is reasonable, we use a simple model of permafrost development beneath the glacier.

In steady state, the permafrost thickness H can be simply calculated from

$$H = \Delta T k / G. \quad (1)$$

The heat flux at the base of the permafrost is equal to the geothermal heat flux, G (approximately 0.06 W m^{-2} in Svalbard [Sclater *et al.*, 1980]). The temperature gradient ΔT is the temperature differential between the surface of the sediment and depth (approximately equal to the mean annual air temperature, which at Bakanin-breen is about -6°C [Hagen *et al.*, 1993]), and we take sediment thermal conductivity k to be $2.04 \text{ W m}^{-1} \text{ K}^{-1}$ [Yoshikawa and Harada, 1995]. Thus equilibrium permafrost thickness for the exposed sediment is 204 m, in agreement with the observations of increasing permafrost thickness at Svea [Gregersen, 1988]. An estimate of the time t taken to form a thickness of permafrost H from unfrozen sediment at 0°C can be obtained from [e.g., Lock, 1990]

$$H = \sqrt{2k\Delta T t / \rho L n}, \quad (2)$$

where ρ is the density of the sediments, 2000 kg m^{-3} , n is the porosity, 0.25, L , the latent heat of fusion for ice, $3.35 \times 10^5 \text{ J kg}^{-1}$. Equation (2) is applicable to the early stages of growth of ice-rich permafrost with zero initial thickness. Assuming the basal temperature at the glacier is -1°C , equation (2) suggests that the 12–13 m of permafrost we believe exists beneath the lower glacier would form in about 190 years, which is in reasonable agreement with the known retreat history of the glacier.

9.3. Is the Glacier Warm-Bedded Up Glacier of the Surge Front?

Up glacier of the surge front a thermistor string (Figure 1) showed the glacier to be warm-bedded in 1995, with $\sim 40 \text{ m}$ of ice at, or very close to, the pressure melting point (Figure 12). These measurements are supported by the low sediment viscosity estimated from plough meter results.

9.4. Is There Sufficient Heat Generation During the Surge to Explain the Thickness and Form of the Scattering Zone?

The energy source for heating the glacier ice by both strain and frictional heating comes from the loss of potential energy. An estimate of the maximum heat available to warm the ice can be made from the volume of ice transferred down glacier. For example, between 1985 and 1986 the front propagated down glacier by $\sim 1700 \text{ m}$, displacing a volume of ice of about $6.7 \times 10^8 \text{ m}^3$ down glacier with an average surface lowering of $\sim 15 \text{ m}$ over a surface area of $\sim 46 \text{ km}^2$ [Murray *et al.*, 1998]. This represents a total energy loss per unit area of $\sim 1.8 \times 10^6 \text{ J m}^{-2}$. If we assume that the ice temperature was at -1°C before the surge, then this energy can raise the temperature of a layer of ice $\sim 1.0 \text{ m}$ thick

over the whole up glacier area to the pressure melting point (taking the specific heat capacity of ice to be $2097 \text{ J kg}^{-1} \text{ K}^{-1}$). If the ice temperature before the surge was closer to the pressure melting point, then a greater thickness of ice can be warmed. However, if some energy is used to warm the permafrost or to produce water within the warm ice, then the thickness of warm ice that can be produced will be reduced. The division of the energy released between warming the ice and melting the bed depends on the thermal properties of ice, and frozen and unfrozen sediment, and the ratio of frictional heat to strain heating of the ice. Assuming the thermal properties of the sediment are identical to the ice, its porosity is 0.25, and all the heat generated melts the bed, then the total energy release calculated above would melt centimetres of permafrost (because of the need to melt the interstitial ice rather than simply warm it). Furthermore, any loss of heat from the bed by purging water and sediments up faults will tend to warm the ice over the bed. Therefore we believe that there will be a zone of warm basal ice, underlain by a thin layer of unfrozen sediments, but that beneath this the permafrost will remain.

Heat production by frictional heating is proportional to the product of the sliding velocity and the basal shear stress [Paterson, 1994, p. 226]. Regions of the glacier where the scattering zone increases in thickness, i.e., corresponding to the trough in the basal reflection located at 1700–1860 m on Longline, should correspond to increases in one of these parameters. Unless the glacier velocity varies significantly on length scales of $\sim 100 \text{ m}$, which seems unlikely, then this region represents an area of increased basal friction, i.e., a “sticky zone” beneath the glacier.

10. Implications for the Surge Mechanism

10.1. Propagation of Surge Front and Mechanics of Surging

Our interpretation ties the current late surge phase position of the surge front with a transition between warm-bedded and cold-bedded regions of the glacier. Down glacier of the surge front the bed is cold; up glacier of the front it is warm, at least at the interface (and indeed, it must have been so in order for fast flow to occur). This is remarkably like the situation in early surge phase, where the 1986 internal reflecting horizon is also believed to represent the transition between cold and warm ice (Figure 2a). The propagation of the surge front appears to have been associated with the down glacier propagation of this warm bed.

As the surge front propagated down glacier, the thickness of new warm bed created must initially have been small because of the time and energy required to melt the permafrost. Thus our interpretation argues for a surge propagated by sliding or by the deformation of

a thin (centimeters to decimeters thick) layer of sediments, rather than by pervasive sediment deformation. The permafrost underlying this thin warm bed will act as a hydrological seal, tending to trap basal water at the interface. The trapped water will help to maintain fast flow by reducing friction and might well be the cause of prolonged active phases of Svalbard glaciers.

10.2. Water Escape and Surge Termination

We have suggested that high-pressure basal water will become trapped in a layer of sediments between the fast moving ice and a seal of impermeable permafrost beneath it (Figure 11). Surge termination requires dissipation of these high basal water pressures, or a substantial reduction in basal shear stress. At Bakaninbreen the glacier has stopped surging, but the 60-m-high surge front means that shear stress remains locally high at the surge front [Porter *et al.*, 1997]. Thus it seems likely that surge termination resulted from a dissipation of basal water pressure.

Basal water can escape from the high-pressure layer in three ways. First, by refreezing at the ice-bed interface. Second, as groundwater through a completely unfrozen part of the bed, which may exist high on the glacier particularly if these regions of the bed were unfrozen before the surge began (Figure 11). Third, through faults to the glacier surface (Figure 11). We interpret the surfaces that have clearly been washed by flowing water down glacier of shear zones as evidence that water has escaped from the feature during the summer months. In winter, any water escaping will tend to refreeze at the ice surface. Such flows tend to form frost mounds and icings [e.g., Liestøl, 1977]. Features that resemble small “pingos” were observed to form in lines just down glacier of the surge front in 1986 and are interpreted as water outflowing from a “leaky” surge front. Furthermore, boreholes were observed to drain through englacial sediment features during 1994 and 1995. There is thus substantial evidence that structural features in the glacier ice can drain water from the bed, and they may thus play a crucial role in surge termination. Any drainage of water through such features will tend to be ephemeral, as features will tend to be closed both by the compressive flow regime at the surge front and by the freezing of water in the cold upper layers of ice. If water and sediment are forced into englacial positions, they will tend to form relatively warm englacial layers and will purge heat from the bed.

We suggest that surge termination results because the surge front “leaks.” Leakage may occur up through the glacier ice largely via structural faults. Refreezing at the ice-bed interface may also remove water from the high-pressure, subglacial system. Some water might additionally diffuse through unfrozen regions of the bed, although the flow path is likely to be very long (Figure 11). All of these processes will tend to be slow rather than abrupt and are likely to prevent any catastrophic

flood event. Thus they are consistent with observations of slowly terminating active phases in the Svalbard archipelago [Dowdeswell *et al.*, 1991].

10.3. Thermal Control of Glacier Surging

Surge mechanisms that are associated with thermal instabilities have been suggested previously, and largely rejected [Robin, 1955; Clarke, 1976]. Objections are based largely on the inability of such mechanisms to explain surges in temperate ice and a desire for a general, unifying surge mechanism [Clarke *et al.*, 1984; Clarke and Blake, 1991]. However, in Svalbard, surging appears to be associated with the presence of internal reflecting horizons in radio echo sounding data [Hamilton and Dowdeswell, 1996; Jiskoot *et al.*, 2000] and our results from Bakaninbreen show a thermal evolution through the active surge phase.

11. Summary and Conclusions

Ground-penetrating radar surveys have produced good imaging of the internal structure of Bakaninbreen and the bed beneath it. We have imaged englacial sediment-filled features that transport significant volumes of sediment, a subhorizontal, basal reflector, which is interpreted as the top of a meters-thick layer of sediment-rich basal ice, and a number of other features within the ice and the bed. Up glacier of the surge front, the basal reflector is overlain by a scattering zone, which is interpreted as warm ice. Down glacier of the surge front, there are two interfaces beneath the basal reflector across which there is an increase in the dielectric coefficient and hence an increase in sediment or water content. The upper of these interfaces is interpreted as the base of the glacier, and the lower is interpreted as the base of frozen sediment. Regions also occur in the subbase where the dielectric coefficient decreases, which we interpret as ice lenses.

1. Bakaninbreen has a soft, sedimentary bed that is partly cold and partly warm during the active surge phase. During late surge phase the location of the warm-cold bed transition appears to be coincident with the geometric expression of the surge front. This spatial relation also appears to have occurred early in the surge. Therefore we believe that propagation of the surge front is associated with the propagation down glacier of the transition between warm- and cold-based ice. Because the surge front propagates more rapidly than the cold bed can completely thaw, basal motion must be restricted close to the ice-bed interface.

2. We have proposed an interpretation that involves surge propagation at Bakaninbreen resulting from sliding or deformation of a thin layer of sediment over a seal of permafrost. The surge front leaks water through structural faults in the glacier. Together with refreezing at the ice-bed interface and/or drainage through unfrozen sediments, this process will tend to result in slowly terminating surges and may thus explain the ob-

servations of long surges and indistinct surge terminations in the Svalbard archipelago.

3. Faulting purges water and sediment (and thus heat) from the glacier bed and may be important in surge termination.

4. Faults within the ice incorporate significant volumes of sediment high into glacier ice. Such faults are ubiquitous in the lower glacier occurring approximately every 60 m. Most features do not reach the ice surface.

Acknowledgments. This research was funded by the NERC (GR3/R9757) and the Royal Society. Purchase of the University of Leeds GPR system was made possible by the Academic Development Fund and the School of Geography, University of Leeds. Personal support to J.W. was provided by a University of Leeds studentship and to P.R.P. and H.J. by School of Geography, University of Leeds, studentships. Jon Guldahl (Norsk Polarinstittutt) assisted greatly with logistics in the field. Brian Davison contributed enormously to the success of our field program. Many of the ideas in this paper were developed while T.M. was on sabbatical at the Department of Earth and Ocean Sciences, University of British Columbia. This paper was improved by constructive reviews by P.U. Clark, A.G. Fountain, W.D. Harrison, and R. Jacobel.

References

- Arcone, S.A., Numerical studies of the radiation patterns of resistively loaded dipoles, *J. Appl. Geophys.*, *33*, 39-52, 1995.
- Arcone, S.A., D.E. Lawson, and A.J. Delaney, Short-pulse radar wavelet recovery and resolution of dielectric contrasts within englacial and basal ice of Matanuska Glacier, Alaska, U.S.A., *J. Glaciol.*, *41*(137), 68-86, 1995.
- Bamber, J.L., Enhanced water scattering from water inclusions in ice, *J. Glaciol.*, *34*(118), 293-296, 1988.
- Bamber, J.L., Ice bed interface and englacial properties of Svalbard ice masses deduced from airborne radio-echo sounding data, *J. Glaciol.*, *35*(119), 30-37, 1989.
- Björnsson, H., Hydrological characteristics of the drainage system beneath a surging glacier, *Nature*, *395*, 771-774, 1998.
- Björnsson, H., Y. Gjessing, S.-E. Hamran, J.O. Hagen, O. Liestøl, F. Pálsson, and B. Erlingsson, The thermal regime of sub-polar glaciers mapped by multi-frequency radio-echo sounding, *J. Glaciol.*, *42*(140), 23-32, 1996.
- Bogorodsky, V.V., C.R. Bentley, and P.E. Gudmansen, *Radioglaciology*, 254 pp., D. Reidel, Norwell, Mass., 1985.
- Clapperton, C.M., The debris content of surging glaciers in Svalbard and Iceland, *J. Glaciol.*, *14*(72), 395-406, 1975.
- Clarke, G.K.C., Thermal regulation of glacier surging, *J. Glaciol.*, *16*(74), 231-250, 1976.
- Clarke, G.K.C., Fast glacier flow Ice streams, surging, and tidewater glaciers, *J. Geophys. Res.*, *92*, 8835-8841, 1987.
- Clarke, G.K.C., and E.W. Blake, Geometric and thermal evolution of a surge-type glacier in its quiescent state: Trapridge Glacier, Yukon Territory, Canada, 1969-89, *J. Glaciol.*, *37*(125), 158-169, 1991.
- Clarke, G.K.C., S.G. Collins, and D.E. Thompson, Flow, thermal structure and subglacial conditions of a surge-type glacier, *Can. J. Earth Sci.*, *21*(2), 232-240, 1984.
- Clarke, G.K.C., J.P. Schmok, C.S.L. Ommanney, and S.G. Collins, Characteristics of surge-type glaciers, *J. Geophys. Res.*, *91*, 7165-7180, 1986.
- Conyers, L.B., and D. Goodman, *Ground-Penetrating Radar: An Introduction for Archaeologists*, 232 pp., Altamira, Walnut Creek, Calif., 1997.
- Davis, J.L., and A.P. Annan, Ground-penetrating radar for high resolution mapping of soil and rock stratigraphy, *Geophys. Prospect.*, *37*, 531-551, 1989.
- Dowdeswell, J.A., G.S. Hamilton, and J.O. Hagen, The duration of the active phase on surge-type glaciers: Contrasts between Svalbard and other regions, *J. Glaciol.*, *37*(127), 338-400, 1991.
- Fischer, U.H., and G.K.C. Clarke, Ploughing of subglacial sediment, *J. Glaciol.*, *40*(134), 97-106, 1994.
- Gregersen, O., Foundation engineering research in Svalbard, in *Svalbard Excursion Guide, 5th International Conference on Permafrost*, edited by A. Orheim and J.L. Sollid, Medd. fra Geografisk Institutt, Univ. Oslo, Naturgeogr. Rapp. 8, Oslo, pp. 26-35, 1988.
- Hagen, J.O., and A. Sætrang, Radio-echo sounding of sub-polar glaciers with low-frequency radar, *Polar Res.*, *9*(1), 99-107, 1991.
- Hagen, J.O., O. Liestøl, E. Roland, and T. Jørgensen, Glacier atlas of Svalbard and Jan Mayern, *Nor. Polarinst. Medd.*, *129*, 141 pp., 1993.
- Hambrey, M.J., J.A. Dowdeswell, T. Murray, and P.R. Porter, Thrusting and debris-entrainment in a surge-type glacier: Bakaninbreen, Svalbard, *Ann. Glaciol.*, *22*, 241-248, 1996.
- Hamilton, G.S., and J.A. Dowdeswell, Controls on glacier surging in Svalbard, *J. Glaciol.*, *42*(140), 157-168, 1996.
- Hobbs, P.V., *Ice Physics*, 837 pp., Clarendon, Oxford, England, 1974.
- Hodgkins, R., Glacier hydrology in Svalbard, Norwegian high arctic, *Quat. Sci. Rev.*, *16*, 957-973, 1997.
- Jiskoot, H., P.J. Boyle, and T. Murray, The incidence of glacier surging in Svalbard: Evidence from multivariate statistics, *Comp. Geosci.*, *24*(4), 387-399, 1998.
- Jiskoot, H., T. Murray, and P.J. Boyle, Controls on the distribution of surge-type glaciers in Svalbard, *J. Glaciol.*, in press, 2000.
- Jones, F.H.M., Digital impulse radar for glaciology: Instrumentation, modelling, and field studies, M.Sc. thesis, 110 pp., Univ. of B. C., Vancouver, 1987.
- Kamb, B., Glacier surge mechanisms based on linked cavity configuration of the basal water conduit system, *J. Geophys. Res.*, *92*, 9083-9100, 1987.
- Lefauconnier, B., and J.O. Hagen, Surging and calving glaciers in eastern Svalbard, *Nor. Polarinst. Medd.*, *116*, 130 pp., 1991.
- Liestøl, O., Pingos, springs and permafrost in Spitsbergen, *Nor. Polarinst. Årbok*, 1975, 7-29, 1977.
- Lock, G.S.H., *The Growth and Decay of Ice*, 434 pp., Cambridge Univ. Press, New York, 1990.
- Macheret, Y.Y., M.Y. Moskalevsky, and E.V. Vasilenko, Velocity of radio waves in glaciers as an indicator of their hydrothermal state, structure and regime, *J. Glaciol.*, *39*(132) 373-384, 1993.
- Meier, M.F., and A. Post, What are glacier surges?, *Can. J. Earth Sci.*, *6*, 807-817, 1969.
- Murray, T., Assessing the paradigm shift: Deformable glacier beds, *Quat. Sci. Rev.*, *16*(9), 995-1016, 1997.
- Murray, T., D.L. Gooch, and G.W. Stuart, Structures within the surge front at Bakaninbreen using ground penetrating radar, *Ann. Glaciol.*, *24*, 122-129, 1997.
- Murray, T., J.A. Dowdeswell, D.J. Drewry, and I. Frearson, Geometric evolution and ice dynamics during a surge of Bakaninbreen, Svalbard, *J. Glaciol.*, *44*(147) 263-272, 1998.
- Ødegard, R.S., J.O. Hagen, and S.-E. Hamran, Comparison of radio-echo sounding (30-1000 MHz) and high-resolution borehole-temperature measurements at Finsterwalderbreen, southern Spitsbergen, Svalbard, *Ann. Glaciol.*, *24*, 262-267, 1997.

- Paterson, W.S.B., *The Physics of Glaciers*, 3rd Ed., 480 pp., Pergamon, Tarrytown, N.Y., 1994.
- Porter, P.R., Glacier surging: Subglacial sediment deformation and ice-bed coupling, Ph.D. thesis, 235 pp., Univ. of Leeds, Leeds, England, 1997.
- Porter, P.R., T. Murray, and J.A. Dowdeswell, Sediment deformation and basal dynamics beneath a glacier surge front: Bakanmbreen, Svalbard, *Ann. Glaciol.*, 24, 21-26, 1997.
- Punning, J.-M., L. Troitskiy, and R. Rajamae, The genesis and age of Quaternary deposits in the eastern part of Van Mijenfjorden, west Spitsbergen, *Geol. Foren. Stockholm Forh.*, 98(567), part 4, 343-347, 1976.
- Robin, G. de Q., Ice movement and temperature distribution in glaciers and ice sheets, *J. Glaciol.*, 2(18), 523-532, 1955.
- Salvigsen, O., and T.S. Wisnes, Braganzavægen, Geological map of Svalbard, scale 1:100 000, C10G, Nor. Polarinst., Oslo, 1989.
- Sclater, J.C., C. Jaupart, and D. Galson, The heat flow through oceanic and continental crust and the heat loss of the Earth, *Rev. Geophys.*, 18, 269-311, 1980.
- Sheriff, R.E., and L.P. Geldart, *Exploration Seismology*, 2nd Ed., Cambridge Univ. Press, New York, 1995.
- Yilmaz, O., *Seismic Data Processing*, SEG Invest. Geophys., no. 2, 1987.
- Yoshikawa, K., and K. Harada, Observations on nearshore pingo growth, Adventadalen, Spitsbergen, *Permafrost Periglacial Processes*, 6, 361-372, 1995.
-
- H. Jiskoot, T. Murray, P. R. Porter and J. Woodward, School of Geography, University of Leeds, Leeds, LS2 9JT, England, U.K. (e-mail: T.Murray@geog.leeds.ac.uk)
- P. J. Miller and G. W. Stuart, School of Earth Sciences, University of Leeds, Leeds, LS2 9JT, England, U.K. (e-mail: G.Stuart@earth.leeds.ac.uk)
- A. M. Smith, Physical Sciences Division, British Antarctic Survey, Natural Environment Research Council, Madingley Road, Cambridge, CB3 0ET, England. (e-mail: amsm@bas.ac.uk)

(Received May 25, 1999; revised February 11, 2000; accepted February 23, 2000.)